High Load Performance and Combustion Analysis of a Four-valve Direct Injection Gasoline Engine Running in the Two-stroke Cycle

Abstract

With the introduction of CO2 emission legislation or fuel economy standards in Europe and many other countries, significant effort is being made to improve spark ignition (SI) gasoline engines because of their dominant market share in passenger cars and potential for better fuel economy. Amongst several approaches, the engine downsizing technology has been adopted by the automotive companies as one of the most effective methods to reduce fuel consumption of gasoline engines. However, aggressive engine downsizing is constrained by excessive thermal and mechanical loads as well as knocking combustion and low speed pre-ignition (also known as super-knock). In order to overcome such difficulties, a gasoline direct injection single cylinder engine was modified to run under the two-stroke cycle by operating the intake and exhaust valves around bottom dead centre (BDC) at every crankshaft revolution. The combustion products were scavenged by means of a reversed tumble flow of compressed air during the positive valve overlap period at BDC. The engine output was determined by the scavenging and trapping efficiencies, which are directly influenced by the intake and exhaust valve timings and boost pressures. In this research a valve timing optimization study was performed using a fully flexible valve train unit, where the intake and exhaust valves were advanced and retarded independently at several speeds and loads. A supercharger was used to vary the load by increasing the boost pressure. The effects of valve timing and boost pressure in the two-stroke cycle were investigated by a detailed analysis of the gas exchange process and combustion heat release. Gaseous and smoke emissions were measured and analysed. The results confirmed that the two-stroke cycle operation enabled the indicated mean effective pressure (IMEP) to reach 1.2 MPa (equivalent to 2.4 MPa of a 4-stroke cycle) with an in-

cylinder pressures below 7 MPa at an engine speed as low as 800rpm. The engine operation was limited by scavenging inefficiencies and short time available for proper air-fuel mixing at high speeds using the current fuel injector. The large amounts of hot residual gas trapped induced controlled auto-ignition combustion at high speeds, and thus the abrupt heat release limited higher loads.

1. Introduction

Two-stroke engines are well known for their superior power density and reduced weight compared to equivalent four-stroke units and are employed to power handheld tools to large marine engines [1][2]. Their use for high performance purposes is widely spread for motorbikes, snowmobiles and outboard vehicles, with claimed power densities above 220 kW/litre [3]. However, these advantages, mainly related to crank-case scavenged two-stroke engines, are often offset by drawbacks regarding gaseous emissions, thermal efficiency and engine components durability [4].

On the subject of emissions, the fuel short-circuiting in mixture scavenged two-stroke engines results in significant unburned hydrocarbon (uHC) emissions. The lubricant added to the fuel has much less effect on emissions from crank-case scavenged two-stroke engines according to [3], as modern units use proportions as low as 1% of oil in the fuel. Regarding the thermal efficiency, conventional two-stroke engines usually lose expansion work in favour of enhanced scavenging through early exhaust port opening. This procedure uses the exhaust blow-down phase to reduce the levels of residual gas trapped prior to the intake process, ensuring higher degrees of charge purity [5]. Lastly, the reduced components durability (piston, rings and liner) of ported two-stroke engines can be attributed to uneven thermal loads and reduced lubricant oil film when uHC emissions is a concern [7]. It is important to keep in mind that all these disadvantages are related to cross-scavenged and loop-scavenged two-stroke engines with intake and exhaust ports, where the crank-case is employed as a pump for the air or air/fuel mixture and therefore lubricant oil needs to be added to the air stream. Such problems can be avoided by the uniflow two-stroke engine concept, in which externally compressed air is supplied through ports at bottom dead centre (BDC) and the exhaust gas is forced out through conventional poppet valves in the cylinder head. Greater scavenging efficiencies can be achieved with such designs [1], but production complexity and packaging restrictions have limited its application to large marine diesel engines so far though some attempts have been made to adopt such an engine design for vehicular applications [8].

In the beginning of 1990 a new concept of two-stroke operation was proposed as a possible solution to overcome the problems of conventional ported two-stroke engines. Based on the design of modern four-stroke engines, the two-stroke scavenging process was achieved through the overlap period of overhead intake and exhaust valves around BDC at every engine revolution [2][7][9]. Because of the use of poppet valves higher power outputs could be achieved with the same engine durability as four-stroke engines. The high levels of uHC emissions due to fuel short-circuiting had been addressed by direct fuel injection and air-assisted fuel injection [5]. The lubricant oil consumption, characteristic of crank-case scavenged engines, had been eliminated by using wet sump and external scavenge pump, mostly roots blower superchargers. When applying this concept to Diesel engines, 40% higher torque and reduced combustion noise compared to an equivalent four-stroke model was demonstrated by Toyota [7].

A reported problem of gasoline direct injection (GDI) two-stroke poppet valve engines was the insufficient mixing between fuel and air in the cylinder, mainly attributed to the shorter time available and the relatively lower injection pressures used at the time [7]. The poor charge mixing resulted in incomplete combustion and large emissions of CO, uHC and soot, as studied by [10]. However, over the last few years significant advances have been made in high pressure fuel direct injection systems and high efficiency boosting devices (superchargers, turbochargers and e-boosters). In addition, flexible variable valve actuation systems, particularly fast variable cam devices, have been developed for production engines [11]. Such technological improvements have prompted renewed interest in developing two-stroke poppet valve gasoline engines [12][13] and diesel engines [14][15], considering their potential for aggressive engine downsizing with lower in-cylinder pressures and less structural stresses than downsized four-stroke engines [16][17]. Moreover, the two-stroke poppet valve engine shares nearly all components from the contemporary four-stroke engine architecture and hence can be produced from the same manufacturing process.

In the previous study [13][18] it was demonstrated that controlled auto-ignition (CAI), or homogeneous charge compression ignition (HCCI), combustion could be used to improve the combustion stability and efficiency at part load conditions in the two-stroke poppet valve engine. Higher efficiencies and near zero oxides of nitrogen (NOx) emission across a wide range of engine operation conditions at part load were achieved, using gasoline and mixtures of gasoline-ethanol.

In order to evaluate the high load potential of the two-stroke direct injection gasoline poppet valve engine operation, the present study was carried out at higher load conditions with increased boost pressures at several engines speeds. The intake and exhaust valve timings were varied and their effects on the scavenging process and engine performance were investigated. Measurements of gaseous and smoke emissions, as well as the heat release analysis, were performed to study the air-fuel mixing and combustion process during the two-stroke cycle.

2. Experiments

2.1 Experimental setup

All the experiments were conducted on a single cylinder research engine mounted on a transient test bed. The engine was equipped with an electro-hydraulic fully variable valve train unit capable of independent control over the timings and lifts of each of the four valves, enabling both two-stroke and four-stroke cycles operation [19]. The engine has an 81.6 mm bore and 66.9 mm stroke, with a geometrical compression ratio of 11.8:1 and a pent roof combustion chamber. The valve control unit operated under closed loop control over oil pressure, temperature and valve timing/lift, ensuring precise valve operation up to 3000 rpm in the two-stroke cycle. A Ricardo rCube engine control unit was used to manage the throttle position, injection pulse width, spark timing and valve parameters. An AC dynamometer enabled both motored and fired operations whilst an external cooling system provided fully automated control over engine oil and coolant temperature. Gasoline (95 RON) was directly injected into the combustion chamber through a side mounted Denso solenoid double-slit type injector [20]. The instantaneous fuel mass flow rate was measured by an Endress+Hauser Promass 83A Coriolis flow meter, with a maximum error of ±0.2% for the flow range studied. The boosted air was supplied by an AVL 515 sliding vanes compressor unit with closed loop control over the pressure. The air mass flow rate was measured by a Hasting HFM-200 laminar flow meter with a maximum error of ±1%. The intake and exhaust pressures were measured by two Kistler piezo-resistive transducers installed in the intake plenum (4007BA20F) and in the exhaust port (4007BA5F), with a maximum error of ±0.1%. The in-cylinder pressure was measured by a Kistler 6061B piezo-electric sensor, with a maximum measurement error of ±0.5%. To record the crank angle positions a LeineLinde incremental encoder with a resolution of 720ppr was employed. Averaged temperatures were measured at the intake plenum, exhaust runner, oil gallery, coolant jacket and fuel rail by using K-type thermocouples with an accuracy of ±1%. An AVL 415SE smoke meter was used to measure the smoke levels, with repeatability better than 3% of the measured value. Gaseous emissions were analysed by a Horiba MEXA 7170DEGR using the non-dispersive infrared principle for CO, a heated flame ionization detector for uHC, a paramagnetic detector for O_2 and a heated chemiluminescence detector for NOx. The overall error attained to each gas measurement was smaller than 2%. The location of all instruments described above can be found in Figure 1, as well as the temperature and pressure measurement points labelled as “T” and “P”, respectively.

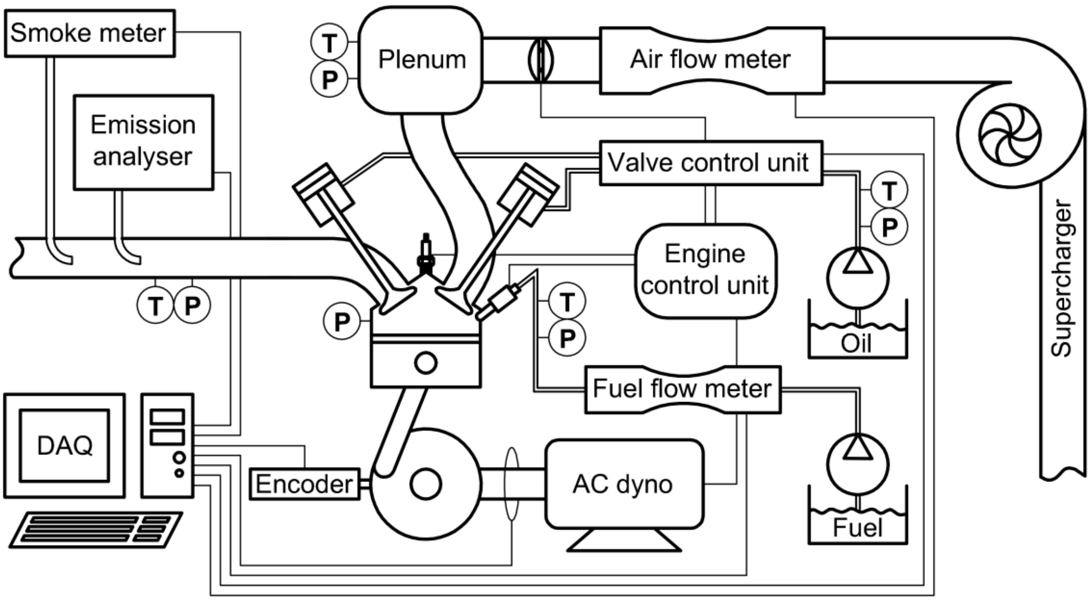

Figure 1 - Research engine and test cell facilities

A National Instruments 6353 USB X card was used for data acquisition (DAQ) and an in-house software was employed for combustion analysis and specific emissions calculations.

2.2 Test procedures

The two-stroke cycle was achieved by opening both the intake and exhaust valves around BDC as presented in Figure 2. The long valve overlap period allowed the inlet boosted air to scavenge the combustion products. The start of fuel injection (SOI) occurred after all the valves were closed to avoid fuel short-circuiting to the exhaust. In addition, SOI after the intake valve closing (IVC) prevented fuel from entering into the intake ports through backflow, which may occur if the in-cylinder pressure becomes higher than the intake port pressure. The fuel entrained in the intake port could then be carried back into the cylinder and pass directly to the exhaust port in the following cycle, contributing to increased uHC emissions.

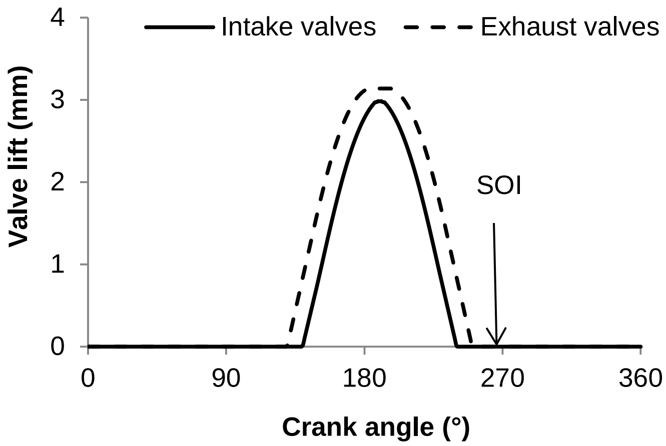

Figure 2 - Two-stroke cycle operation principle

At each of the engine speeds studied, i.e. 800, 1500, 2200 and 3000±5 rpm, five intake pressure levels were applied (where possible) as a way to control the engine load. By increasing the boost pressures from 120±2 kPa to 280±3 kPa the scavenge ratio increased and less residual gas was trapped, resulting in greater air mass in the cylinder and higher engine power output. At some operation points stable combustion was not achieved as the covariance of the indicated mean effective pressure (COV_{IMEP}) reached a limit of 10%. This value seems high for four-stroke engines where a value around 5% is usually considered [21]. However, bearing in mind the doubled firing frequency of two-stroke engines the torque variation is reduced and the levels of vibration and harshness are attenuated. In a previous study, stable operation in a two-stroke poppet valve engine was claimed at COV_{IMEP} values as high as 35% [5].

At each engine speed, nine different combinations of intake and exhaust opening/closing timings were tested as shown in Figure 3 and Figure 4. The intake and exhaust valve durations were kept constant at 100° CA and 120° CA, respectively. At each engine speed and a given boost pressure, the exhaust valve timing was kept fixed and the inlet valve opening (IVO) was varied from 130° CA to 150° CA after top dead centre (ATDC), in steps of 5° CA. Then, the intake valve timing was fixed and the exhaust valve opening (EVO) was varied from 120° CA to 140° CA ATDC, also in steps of 5° CA.

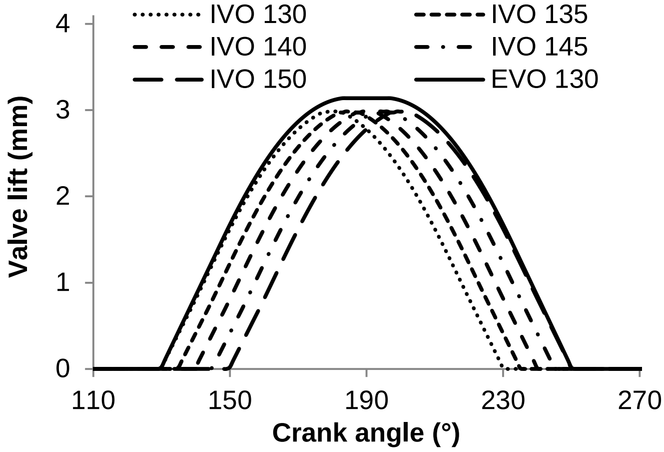

Figure 3 - Intake valve timing optimization

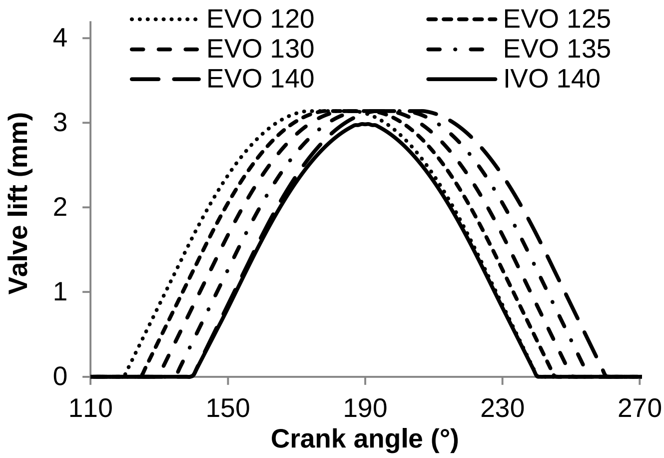

Figure 4 - Exhaust valve timing optimization

In the previous research at part-load conditions [22] the EVC took place before the IVC to increase the residual gas trapped for CAI combustion. In this study, however, the EVC was delayed to obtain higher scavenging efficiencies. In addition, the exhaust valve opened earlier during the expansion process to increase the exhaust blow-down period. During the experiments the maximum advance of IVO was set to the EVO.

To ensure the same air-fuel mixing conditions for all the valve timings studied the SOI was set to 260° CA ATDC, which was the latest EVC timing. During the engine experiments, the fuelling rate was determined for a given engine speed and boost pressure and kept constant when the valve timings were changed. The fuel injection pressure was set to 15.0±0.5 MPa, and its temperature kept at 293±5 K.

The engine coolant and oil temperatures were kept at 353±3 K for all cases studied. The intake air temperature was in the range from 295 K to 305 K, except for the maximum intake pressure at 800 rpm when it reached 325 K due to insufficient air cooling.

The ignition timing was set to minimum spark advance for maximum brake torque (MBT) or knock limited spark (KLS) at conditions when knocking combustion occurred. A knocking combustion threshold of 1 MPa/°CA was set for the maximum rate of pressure rise (dP/dθ).

2.3 Data analysis

Based on the in-cylinder pressure and crank-angle measurements, the mass fraction burnt was calculated according to the Rassweiler-Withrow method presented in [6]:

$$\frac{dQ_{net}}{d\theta} = \frac{\gamma}{\gamma-1}p\frac{dV}{d\theta}+\frac{1}{\gamma-1}V\frac{dp}{d\theta} \qquad (1)$$

Where: Q_{net} is the net heat release, θ is the crank angle, γ is the ratio of specific heats (considered constant and equal to 1.33), p is the in-cylinder pressure and V is the in-cylinder volume.

Exhaust emissions were converted from parts per million (ppm) to g/kWh based on the UN Regulation N49 [23]:

$$ISgas = \frac{u_{gas} c_{gas} \dot{q}_{exh}}{P_i} \tag{2}$$

Where: $ISgas$ is the indicated specific gas emission (CO, HC or NOx), u_{gas} is the specific gas constant (CO = 0.000966, HC = 0.000499 and NOx = 0.001587) for gasoline fuelled engines, c_{gas} is the gas concentration in the exhaust stream, $\dot{q}_{exh}$ is the exhaust mas flow rate and P_i is the indicated power output.

The combustion efficiency was calculated based on the emissions products not fully oxidized during the combustion:

$$\eta_c = 1 - \frac{\dot{m}_{CO} LHV_{CO} + \dot{m}_{HC} LHV_{HC} + \dot{m}_{H_2} LHV_{H_2}}{\dot{m}_{fuel} LHV_{fuel}} \tag{3}$$

Where: η_c is the combustion efficiency, $\dot{m}_{CO}$ is the mass flow rate of CO, LHV_{CO} is the lower heating value (LHV) of CO (10.1MJ/kg), $\dot{m}_{HC}$ is the mass flow rate of uHC, LHV_{uHC} is the LHV of uHC (44MJ/kg), $\dot{m}_{H_2}$ is the mass flow rate of H_2, LHV_{H_2} is the LHV of H_2 (120MJ/kg), $\dot{m}_{fuel}$ is the fuel mass flow rate and LHV_{fuel} is the LHV of the fuel (44MJ/kg).

Emissions of hydrogen (H_2) were estimated based on the measurements of CO and CO_2 according to [24]:

$$[H_2] = \frac{0.5\, y\, [CO]\, ([CO] + [CO_2])}{[CO] + 3\, [CO_2]} \tag{4}$$

Where: $[H_2]$ is the exhaust concentration of hydrogen, y is the hydrogen to carbon ratio of the fuel (considered 1.87), $[CO]$ is the exhaust concentration of carbon monoxide and $[CO_2]$ is the exhaust concentration of carbon dioxide.

The air trapping efficiency, defined as the ratio of in-cylinder trapped air mass to the total intake air mass, was calculated based on the analytical method developed for fuel rich and stoichiometric combustion in two-stroke engines [25]:

$$Trap_{eff(A)} = \frac{0.5[CO] + [CO_2] + 0.25\left(\frac{yK[CO_2]}{[CO] + K[CO_2]}([CO] + [CO_2])\right) + 0.5[NOx]}{0.5[CO] + [CO_2] + [O_2] + 0.25\left(\frac{yK[CO_2]}{[CO] + K[CO_2]}([CO] + [CO_2])\right) + 0.5[NOx]} \quad (5)$$

Where: $Trap_{eff(A)}$ is the air trapping efficiency, $[CO]$ is the exhaust concentration of carbon monoxide, $[CO_2]$ is the exhaust concentration of carbon dioxide, y is hydrogen to carbon ratio of the fuel (considered 1.87), K is the water-gas reaction equilibrium constant (considered 3.5), $[NOx]$ is the exhaust concentration of oxides of nitrogen and $[O_2]$ is the exhaust concentration of oxygen.

Due to the air short-circuiting from the intake to the exhaust during the valve overlap period, the measured exhaust lambda value differed from the in-cylinder lambda. The in-cylinder lambda was then calculated based on the air trapping efficiency and fuel trapping efficiency [25]:

$$\lambda_{in-cylinder} = \lambda_{exhaust} \frac{Trap_{eff(A)}}{Trap_{eff(F)}} \quad (6)$$

Where: $\lambda_{in-cylinder}$ is the in-cylinder lambda, $\lambda_{exhaust}$ is the exhaust lambda, $Trap_{eff(A)}$ is the air trapping efficiency and $Trap_{eff(F)}$ is the fuel trapping efficiency.

The fuel trapping efficiency (defined as the ratio of trapped fuel mass to the total injected fuel mass) in a GDI engine is expected to be 100%, where no fuel short-circuiting is supposed to happen. However, due to the high levels of fuel stratification resulted from the short time available for air-fuel mixing at high speeds and loads, some of the fuel could not take part in the combustion process and left the cylinder unburned. Thus, the fuel trapping efficiency was introduced to take into account the short-circuited fuel from the previous cycle, similar to that used in conventional ported two-stroke engines [25]:

$$Trap_{eff(F)} = \frac{[CO] + [CO_2]}{[CO] + [CO_2] + [uHC]} \tag{7}$$

Where: $Trap_{eff(F)}$ is the fuel trapping efficiency, $[CO]$ is the exhaust concentration of carbon monoxide, $[CO_2]$ is the exhaust concentration of carbon dioxide and $[uHC]$ is the exhaust concentration of unburned hydrocarbons.

The scavenging efficiency, described as the ratio of delivered air mass retained in the cylinder charge to the total in-cylinder charge, was used to indicate how efficiently the burned gases were displaced during the scavenging process. It can be calculated based on the air trapping efficiency and scavenge ratio, as follows:

$$Scvg_{eff} = Trap_{eff(A)} \left(\frac{m_{air}}{Sw_{vol}\rho_{air}}\right) \tag{8}$$

Where: $Scvg_{eff}$ is the scavenging efficiency, $Trap_{eff(A)}$ is the air trapping efficiency, m_{air} is the delivered air mass per cycle, Sw_{vol} is the engine swept volume and ρ_{air} is the air density at ambient conditions. The term between brackets in equation (8) is the scavenge ratio (or delivery ratio), which compares the current delivered air mass per cycle to the reference mass in an ideal charging process.

3. Results and Discussion

3.1 Performance and combustion analysis

The results presented here are averaged over 100 consecutive cycles and plotted as a function of valve timings at given engine speeds and intake pressures. The nomenclature of the different valve timings studied consists of the IVO and the EVO timings in °CA ATDC. The Y-axis is further divided into four parts according to the engine speed. When possible, second and third order polynomial curves were used to fit the date acquired.

Figure 5 shows the maximum IMEP values at different engine speeds and boost pressures. It is noted that higher boost operations were not possible at higher speeds (2200 rpm and 3000 rpm) due to violent combustion and unstable combustion. When the fuelling rate was reduced to avoid excessive heat release rate at higher boost pressure, unstable combustion occurred as measured by the higher COV_{IMEP} values. On the other hand, when the fuelling rate was increased to avoid unstable combustion, the $dP/d\theta$ rose above the knock limit. The occurrence of violent combustion or unstable combustion was likely related to the large amount of hot residual gas trapped, resulted from insufficient time available for scavenging at higher engine speeds. The presence of hot residual gas raised the charge temperature and accelerated the occurrence of auto-ignition combustion in the unburned mixture, resulting in rapid and violent heat release rate. In addition, since the SOI took place at 260° CA ATDC (similar to that of the late injection stratified charge operation in four-stroke GDI engines), significant fuel stratification could be present. If the fuelling rate was reduced, the fuel stratification effect would become more prominent increasing the cyclic variation of the mixture strength around the spark plug. Since the current fuel injection and combustion system were not optimised for the stratified charge operation, larger cycle-to-cycle variations could be expected to occur with greater fuel stratification.

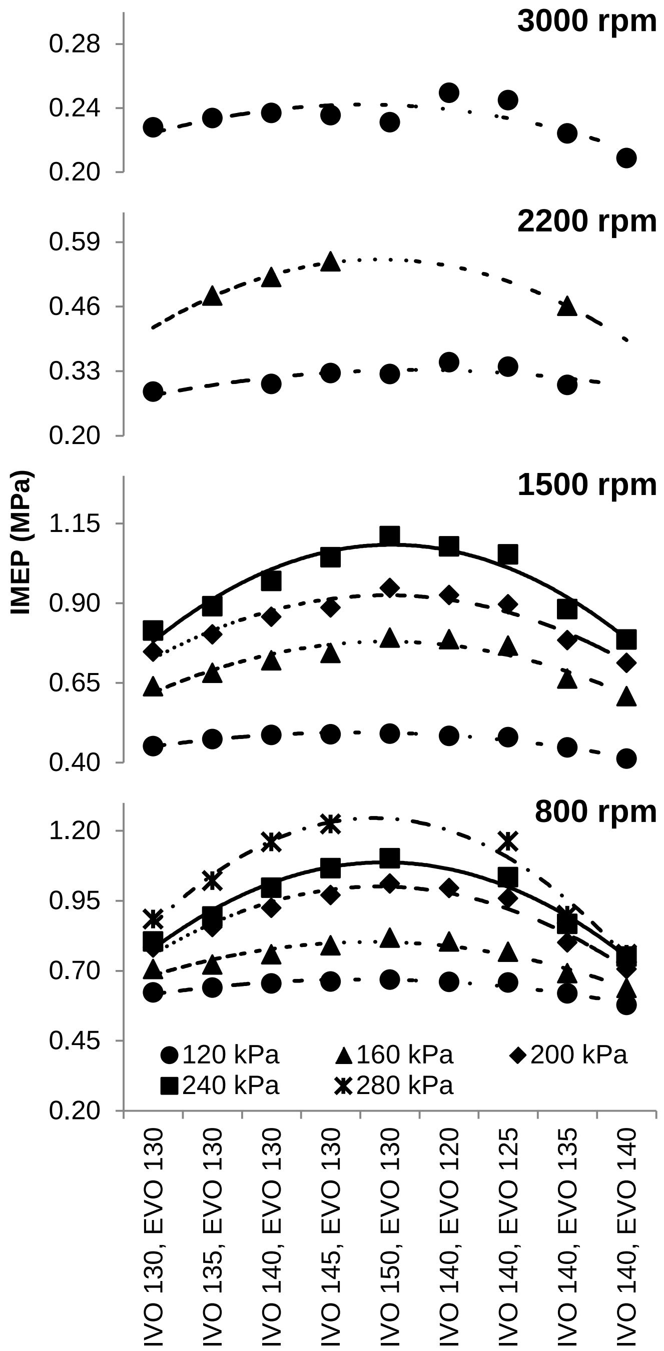

Figure 5 – Indicated mean effective pressure

At 800 rpm all the boosting levels could be tested throughout the valve timings studied except for the latest IVO (150° CA) and earliest EVO (120° CA), when combustion became excessively unstable. From the left to the middle point along the x-axis the IVO was retarded from 130 to 150° CA ATDC at a constant EVO of 130° CA ATDC. At the lowest boost pressure of 120 kPa the IMEP values varied little with IVO. When the boost pressure was higher than 160 kPa, the IMEP increased with the retarded IVO and reached its peak at IVO 150° CA ATDC. It is noted that the higher the boost pressure the more pronounced is the change in IMEP with IVO. This can be explained by an increase in the scavenging efficiency as presented in Figure 6, resulted from higher pressure difference between the intake and exhaust ports. When the IVO was retarded, a more effective blow-down event without intake air contamination was allowed. Such effect would be even more pronounced at higher boost pressures. At 1500 rpm the IVO and EVO sweeps had similar effects on the IMEP, but no stable combustion could be achieved at the boost pressure of 280 kPa.

From the right to the middle along the x-axis in Figure 5 and Figure 6, when the EVO was advanced from 140 to 120° CA ATDC and the IVO kept at 140° CA ATDC, the scavenging efficiency (and therefore the IMEP) changed little at lower boost pressures but rose steadily to reach its peak at the middle of the graph. This behaviour mirrored the left part of the curve and can be explained by the increased blow-down period and higher pressure ratio across the exhaust valves at an earlier EVO. In addition, the difference between the intake air pressure and the in-cylinder burned gases was greater at the same IVO as the in-cylinder pressure had dropped to a lower value due to extended exhaust blow-down.

At 800 rpm the peak IMEP of 1.2 MPa was achieved at an intake pressure of 280 kPa, producing a specific torque of 195 Nm/l with the in-cylinder peak pressure as low as 6.8 MPa. To produce the same torque at the same speed in a four-stroke engine of the same displacement, the engine would need to be operated at 2.4 MPa IMEP. This could only be achieved with twice the in-cylinder pressure (13.6 MPa), assuming the engine would not be limited by knocking combustion and/or low speed pre-ignition (LSPI) inducing super-knock [26].

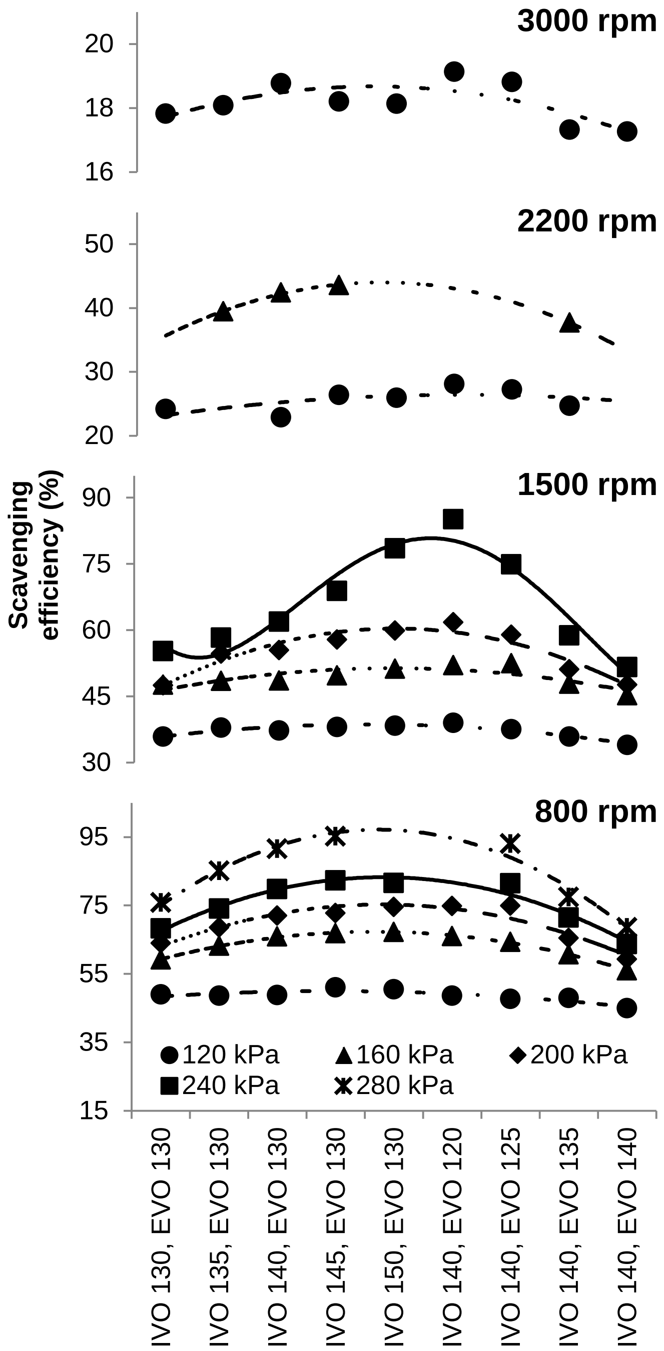

Figure 6 - Scavenging efficiency

The results in Figure 6 illustrate that the maximum IMEP was a direct result of the most completed scavenging process achieved at the latest IVO (150° CA ATDC) and earliest EVO (120° CA ATDC). Because the fuelling rate was kept constant at a given intake pressure, it would have been possible to achieve even higher engine power outputs by increasing the fuelling rate at these valve timings at 800 rpm. However, it would have been at the expense of poorer combustion efficiency and higher fuel consumption. At any given IVO and EVO timings the scavenging efficiency dropped with the increased engine speed because of the reduced time available for gas exchanging. For instance, at 2200 rpm and 120 kPa the residual gas level was found around 75%, whilst at 3000 rpm it reached 82%. Furthermore, at each engine speed the scavenging efficiency decreased from the middle to the both sides of the x-axis, reaching a minimum when the valves opened at the same time, i.e. “IVO 130, EVO 130” and “IVO 140, EVO 140”. In order to better understand the scavenging results, the pressure-volume (P-V) diagrams of four valve timings at 800rpm and 200kPa are plotted in Figure 7.

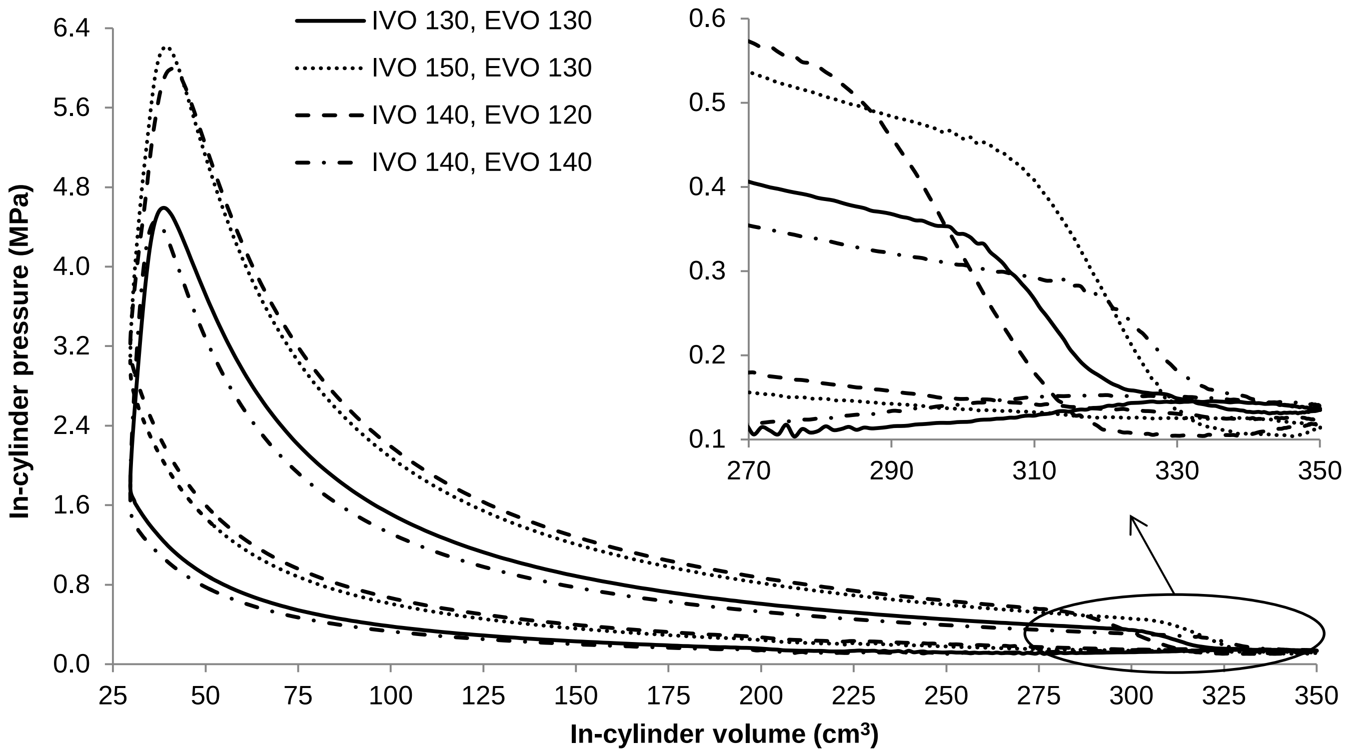

Figure 7 - Pressure-volume diagram for selected valve timings at 800 rpm and 200 kPa

It can be seen from the P-V diagram that the largest amount of useful work was achieved with the earliest EVO (120° CA ATDC) and the latest IVO (150° CA ATDC), when the scavenging process was optimized and less residual gas was trapped. As the valve timing was moved towards “IVO 130, EVO 130”, the greater charge dilution promoted by the internal EGR reduced the heat release rate and hence the peak pressure. It can be seen that in this case the intake and exhaust valves opened at the same time, part of the burned gases mixed with the intake charge and thus compromised the scavenging during the next cycle. The valve timing “IVO 140, EVO 140” was characterised with even lower in-cylinder peak pressure as a result of greater amounts of residual gas trapped, as shown by the lower scavenging efficiency (Figure 6). As shown by the zoomed part of the P-V diagram in Figure 7, in this case the EVO was the most retarded and the expansion loop was the longest amongst those shown. These two extreme valve timings also showed the highest in-cylinder pressures around BDC, which caused the poor scavenging as the pressure drop between intake and exhaust decreased. Moreover, the in-cylinder pressure at the end of the compression phase for these two cases was about 50% lower than that for “IVO 150, EVO 130” and “IVO 140, EVO 120”, resulted from less trapped fresh air mass and higher levels of residual gas with larger heat capacity.

The two valve timings with the highest in-cylinder pressures, i.e.: “IVO 150, EVO 130” and “IVO 140, EVO 120”, presented similar peak pressures (less than 4% of difference), although the early EVO case had reduced useful work and hence 2% lower IMEP. At this speed it is possible to confirm that the exhaust blown-down phase can be partially replaced by a later EVO (130°) with improved expansion work, without compromising the purity of the charge. For this two valve timings the difference in scavenging efficiency was less than 0.5% (Figure 6), whilst the IMEP increased by 2% with later EVO (Figure 5).

The gas exchange process in this two-stroke poppet valve engine was also affected by the actuation speed of the hydraulic valve train. As shown in Figure 8, the valve opening and closing slopes became less steep as the engine speed increased, resulting in reduced effective flow area. Such limitation of the camless system can be overcome by using a conventional camshaft of higher lift driven by the crankshaft at the same speed.

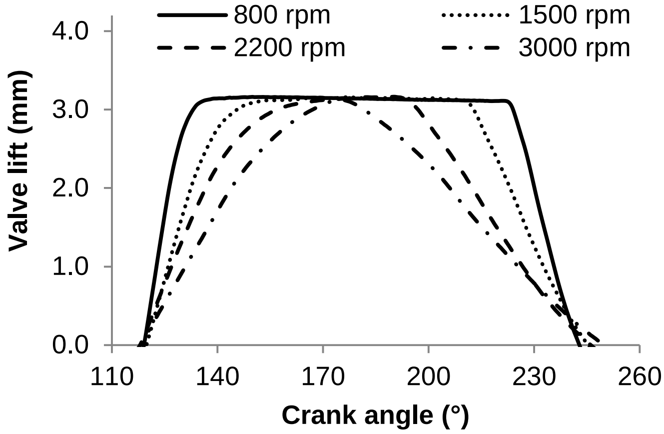

Figure 8 - Effect of engine speed on valve opening and closing durations

Whilst the scavenging efficiency measured the effectiveness of the removal of burned gas, the air trapping efficiency was calculated to determine the air short-circuiting rate. As shown in Figure 9, the trapping efficiency rose steadily with the engine speed as a result of shorter time available for gas exchanging and consequent lower air short-circuiting rate. Higher trapping efficiencies were found for earlier EVO and hence earlier EVC, particularly at 2200 rpm and 3000 rpm, when the overlap period was reduced.

It is noted that when the intake air pressure was set at 120 kPa the air trapping efficiency at 800rpm and 1500 rpm exhibited different trends from the other pressures. This different pattern may be attributed to a transition from a displacement scavenging process to a mixing dominated scavenging process, as idealised by the Benson-Brandham two-part model for gas exchanging in two-stroke engines [27]. According to this theory the scavenging was firstly dominated by a displacement process until it reached a certain value of scavenge ratio, which in this case is around 1.5 at 800 rpm and 0.6 at 1500 rpm. After this point the fresh air and the burned gases were more prone to mix until the end of the scavenging process.

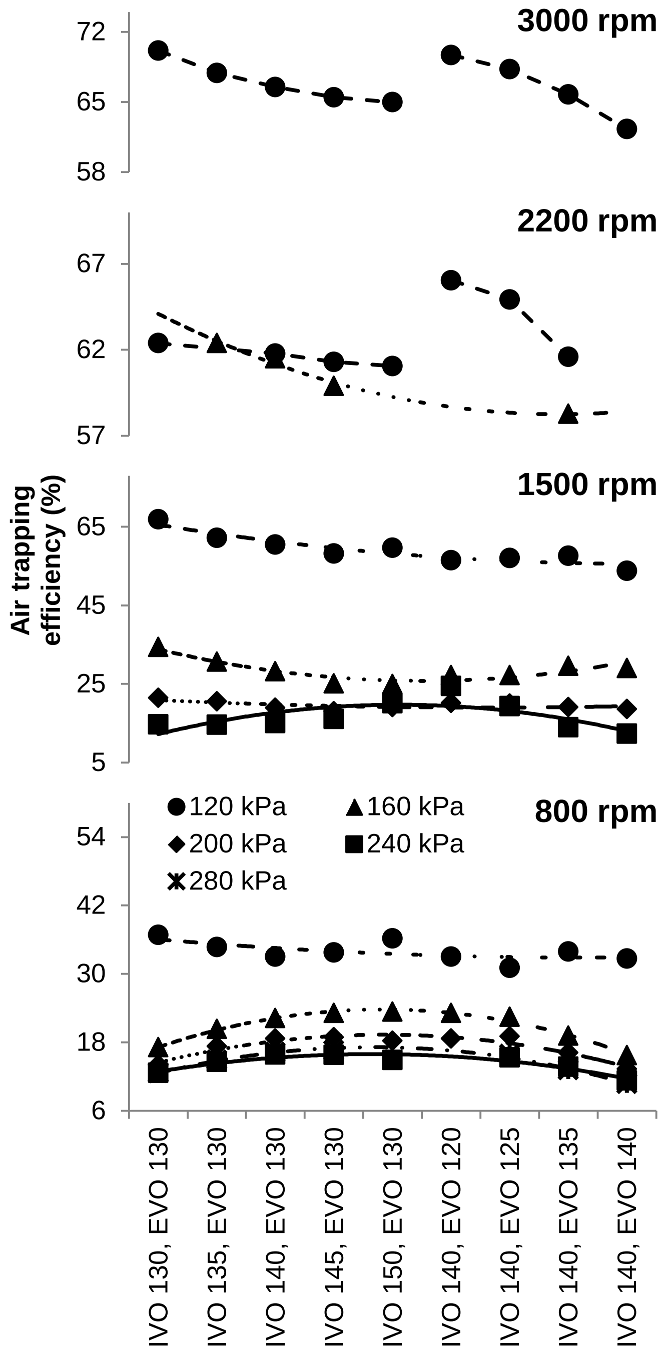

Figure 9 - Air trapping efficiency

The combustion duration, calculated from 10% to 90% of the mass fraction burned (MFB), is presented in two parts according to the intake pressures: the first part for 120/160 kPa (Figure 10) and the second part for 200/240/280 kPa (Figure 11).

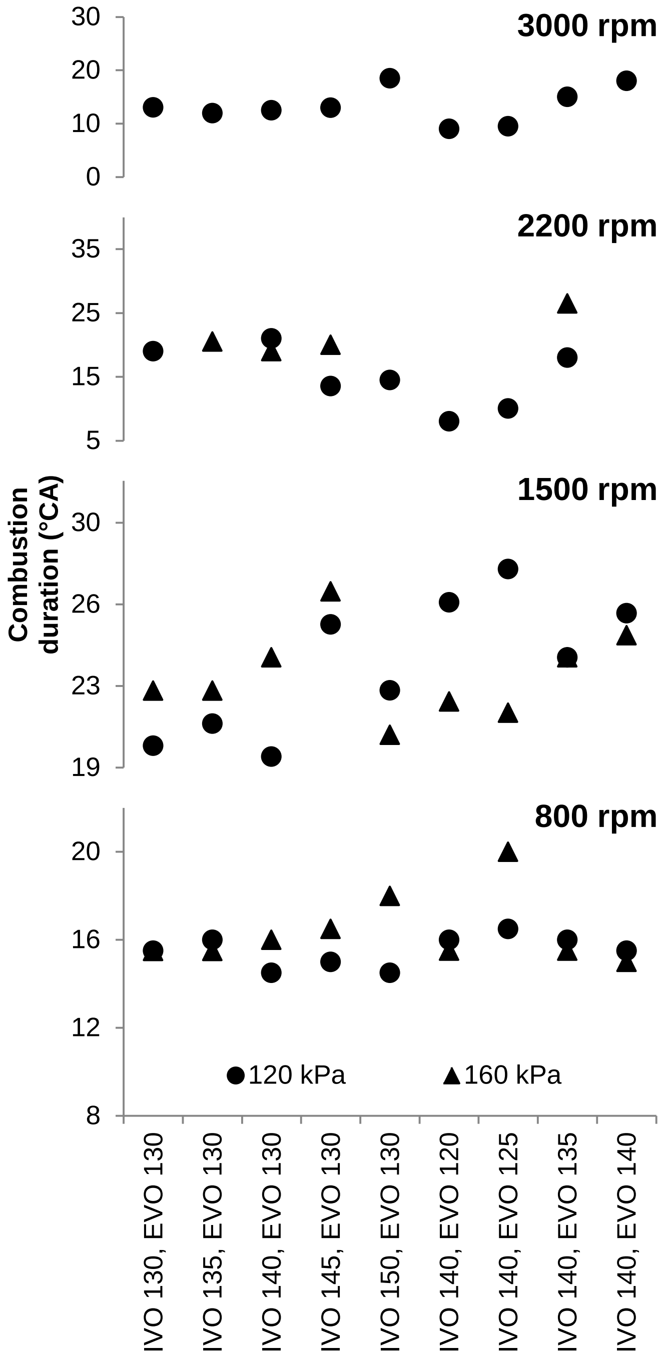

Figure 10 - Combustion duration for 120 kPa and 160 kPa intake pressure

At 800 rpm it is noted that the combustion durations decreased slightly as the boost pressure and load increased because of the higher charge temperatures and pressures. In addition, it can be seen from Figure 10 and Figure 11 that the combustion duration was between 13° CA and 19° CA at 800 rpm, which is much shorter than that of spark ignition (SI) combustion in four-stroke engines. This suggests that the heat release process might have taken place in the form of a spark ignited flame around the spark plug and auto-ignition combustion of some premixed charge in the end-gas [28]. As the engine speed went up to 1500 rpm the combustion duration increased in terms of crank angles, but decreased slightly in absolute time as the flame speed was accelerated by the higher flow turbulence and the auto-ignition combustion was favoured by the hotter residual gas.

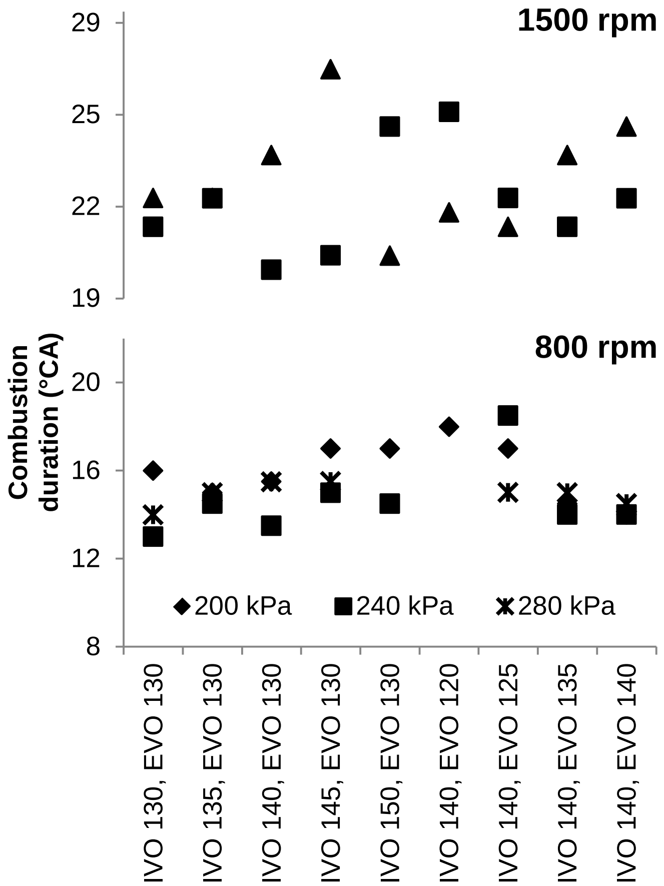

Figure 11 - Combustion duration for 200 kPa, 240 kPa and 280 kPa intake pressure

At 2200 and 3000 rpm stable engine operation was mainly limited to the boost pressure of 120 kPa. During such operation it was found that the spark timing had little effect on the combustion phasing and auto-ignition combustion became the dominant heat release process as evidenced by the very short combustion durations. The combustion duration remained nearly independent of the IVO variation when the EVO was set to 130° CA ATDC. In comparison, the EVO had a more pronounced effect on the combustion duration as shown by the earliest EVO (120° CA ATDC) producing the shortest burning duration.

Figure 12 and Figure 13 show the spark timings set for MBT (black symbols) or KLS (grey symbols) at 800 rpm and 1500 rpm, above which CAI combustion took place and the spark timing had no effect whatsoever. It is noted that the presence of KLS at 1500 rpm was about 50% greater than that at 800 rpm as a result of poorer scavenging efficiencies at higher speeds. In addition, it can be seen that the most retarded KLS occurred at the earliest EVO because of the minimum residual gas concentration as evidenced by the highest scavenging efficiency (Figure 6). For the same reason, the KLS timing became more retarded when the IVO was moved from 130 to 150 °CA ATDC and less residual gas was trapped. When the boost pressure was set to 120 kPa, MBT could be achieved for all the valve timings and more advanced MBT timings were realized near the middle of the x-axis, when both the scavenging efficiency and trapping efficiency were maximized.

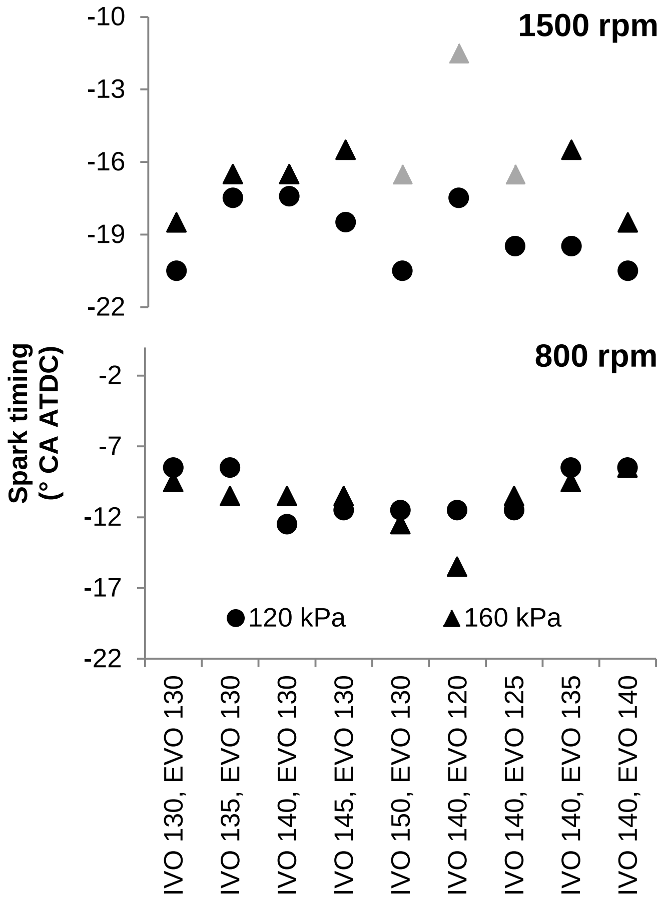

Figure 12 - Spark timings set for MBT (black symbols) or KLS (grey symbols) for 120 kPa and 160 kPa intake pressure

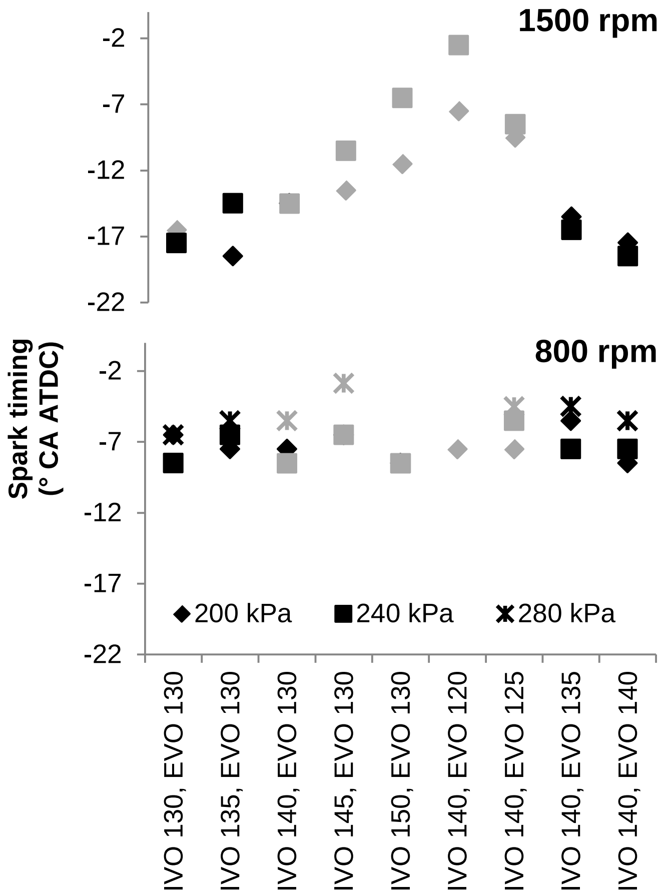

Figure 13 - Spark timings set for MBT (black symbols) or KLS (grey symbols) for 200 kPa, 240 kPa and 280 kPa intake pressure

Figure 14 shows that a minimum ISFC of 255 g/kWh was achieved at 800 rpm and IVO 150° / EVO 120° CA ATDC for all the boost pressures. Although the minimum ISFC was achieved at the same valve timing at 1500rpm, its value increased with higher boost pressures. In order to better understand the ISFC results, it is necessary to look at the valve timing effect over the compression and expansion process, as well as the in-cylinder mixture composition and combustion.

Considering that the indicated specific fuel consumption is intrinsically linked to the expansion work, scavenging efficiency and combustion efficiency, there is a trade-off between higher scavenging rates through exhaust blow-down with early EVO and higher expansion works with late EVO. This effect is clearer in Figure 15, where the effective compression ratio (ECR) and effective expansion ratio (EER) are plotted as a function of the valve timings.

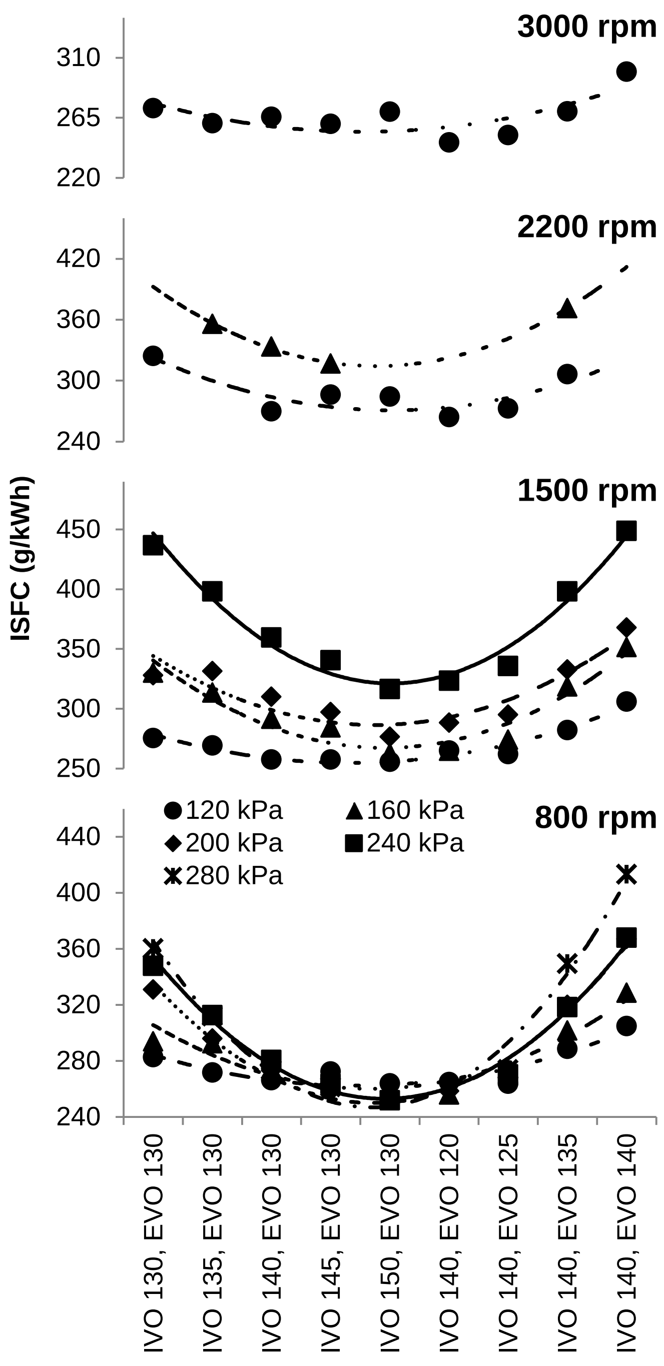

Figure 14 - Indicated specific fuel consumption

Figure 15 shows that for a given exhaust valve timing both the effective compression and expansion ratios were constant and the EER was higher than the ECR by about one. The effective compression and expansion ratios matched each other at “IVO 140, EVO

120”, and when the EVO was retarded from 120° to 140° CA ATDC the EER increased and the ECR was reduced. The highest EER and hence highest expansion work was achieved with the most retarded EVO. However, such an increase in the useful work by the higher EER did not result in improved ISFC.

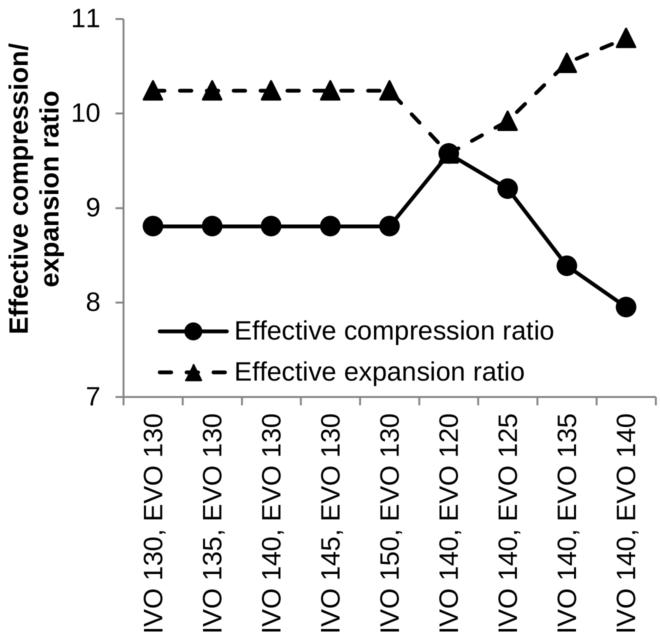

Figure 15 - Effective compression and expansion ratios

The most significant cause for the change in ISFC as a function of valve timings was found from the combustion efficiency plots in Figure 16. It can be seen that the combustion efficiency results mirrored exactly those of ISFC presented in Figure 14. The highest combustion efficiencies and lowest ISFCs occurred in the middle of the graphs around “IVO 150, EVO 130” / “IVO 140, EVO 120” and at 800 rpm. The combustion efficiency decreased with higher engine speeds at the same boost pressure, and it dropped with higher boost pressures at each engine speed.

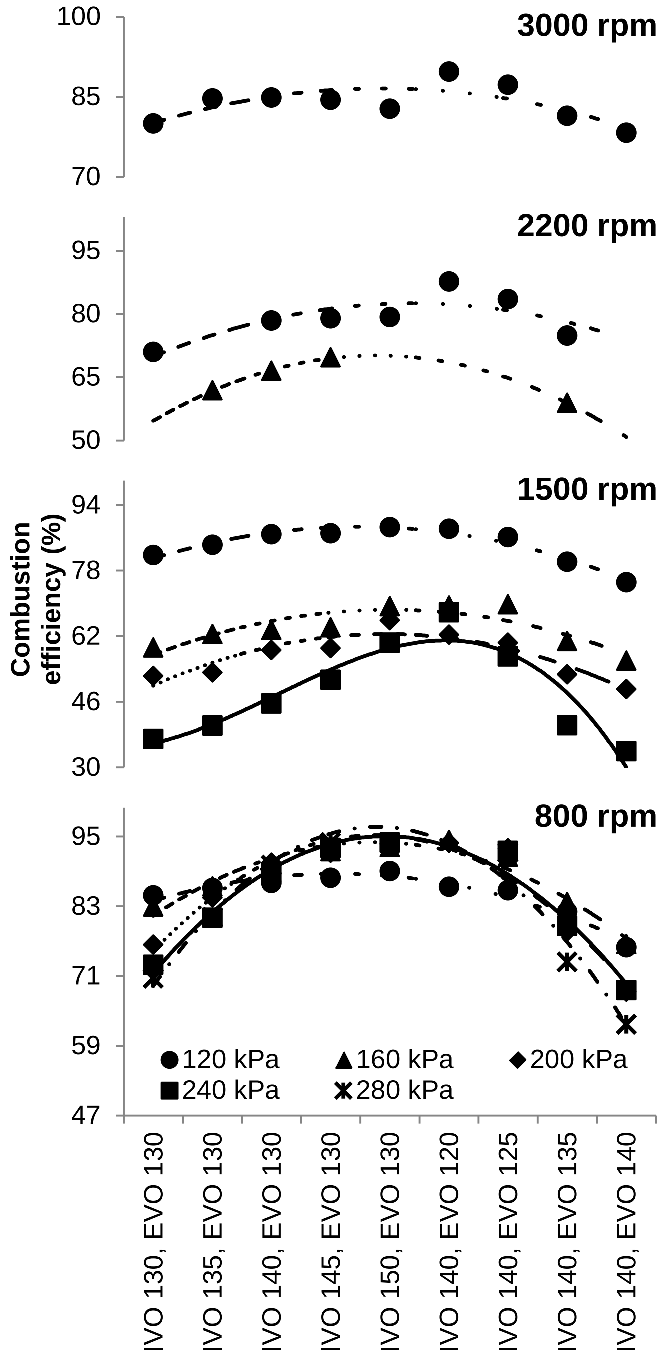

Figure 16 - Combustion efficiency

As shown by the in-cylinder lambda values in Figure 17, the change in combustion efficiency with valve timings can be attributed to the variation of in-cylinder air/fuel mixture with the gas scavenging process. The higher the relative air/fuel ratio (lambda) the more complete the combustion became. The leanest mixture of near stoichiometric air/fuel ratio was reached at 800rpm and resulted in a combustion efficiency of 94%. As the engine speed was increased from 800rpm to 2200rpm, the decreased scavenging efficiencies led to richer air/fuel mixtures and lower combustion efficiencies. At the lowest boost pressure of 120kPa, the combustion efficiency became higher at 3000rpm than 2200rpm mainly because of the leaner mixture and faster heat release rate (Figure 10).

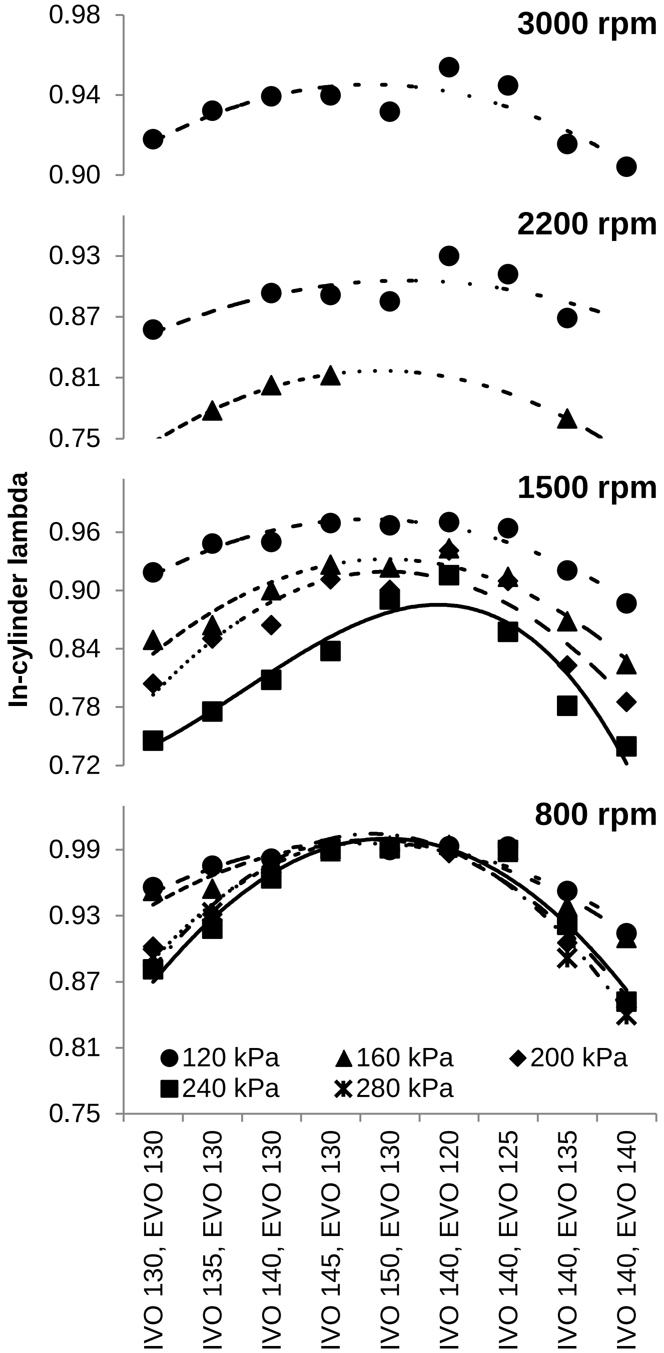

Figure 17 - In-cylinder lambda

3.2 Emission analysis

As shown in Figure 18, CO emission increased significantly as the mixture became richer with more advanced IVO or retarded EVO at each engine speed. Figure 18 shows that negligible CO emission was produced at 800 rpm when the scavenging efficiency and lambda were maximised. Based on the estimated in-cylinder lambda results in Figure 17, some noticeable CO emission was expected by combustion of the slightly overall fuel rich mixture. The lower than expected CO emission could be caused by the oxidation of CO to CO_2 by the short-circuited air mixed with the burned gas during the scavenging process. As the engine speed was increased from 800rpm to 2200rpm, the poorer scavenging and combustion of richer mixtures resulted in significant increase in CO and uHC emissions at higher engine speeds. In addition, the mixture would be less homogeneous at higher engine speed because of the reduced time available between the end of injection and the beginning of combustion. This could have contributed to the very rapid rise in CO emissions when the engine speed was changed from 800rpm to 1500rpm.

As shown in Figure 19, uHC emission showed less dependency on valve timings and lower correlation with the scavenging efficiency and in-cylinder lambda. As late injections were employed, most uHC emissions were likely produced by the fuel rich combustion as well as fuel impingement due to retarded injection. The uHC emissions will not only dependent on the overall air/fuel ratio but also its homogeneity. As injection took place after 260° CA ATDC, there was limited time available for a homogeneous mixture to form. Very rich mixtures could be present in some regions producing uHC emissions. In addition, at higher loads and boost pressures, the end of injection could be as late as 290 ° CA ATDC, when the piston was only at about 25 mm from the cylinder head. Thus, the fan shaped spray impinged onto the piston and formed pool fires on it top. For the same reasons, high smoke emissions were observed as seen in Figure 20. Compared to uHC emissions, the smoke emission was noticeably more affected by the load and speed as the fuel impingement increased with longer injection durations.

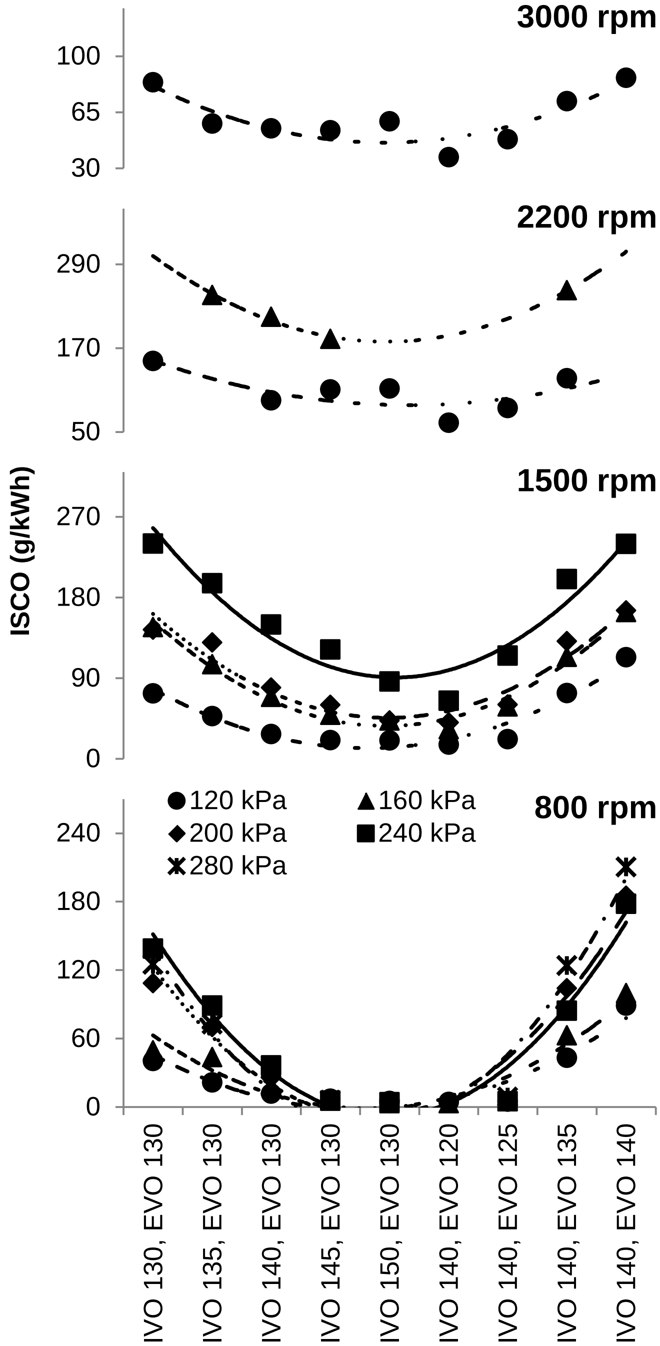

Figure 18 - Carbon monoxide emissions

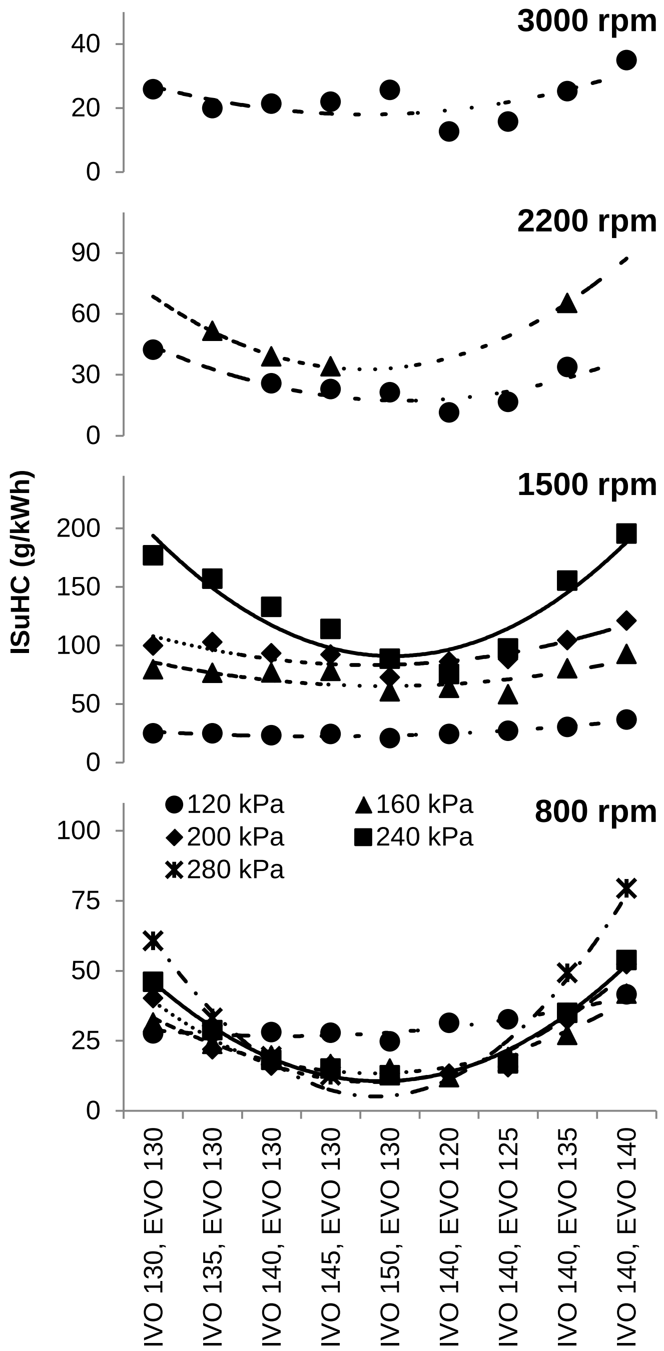

Figure 19 - Unburned hydrocarbon emissions

Furthermore, at the lowest boost pressure of 120kPa both CO and uHC emissions and smoke levels were less at 3000rpm than 2200rpm. It is attributed to the leaner mixture and faster heat release rate as shown in Figure 10.

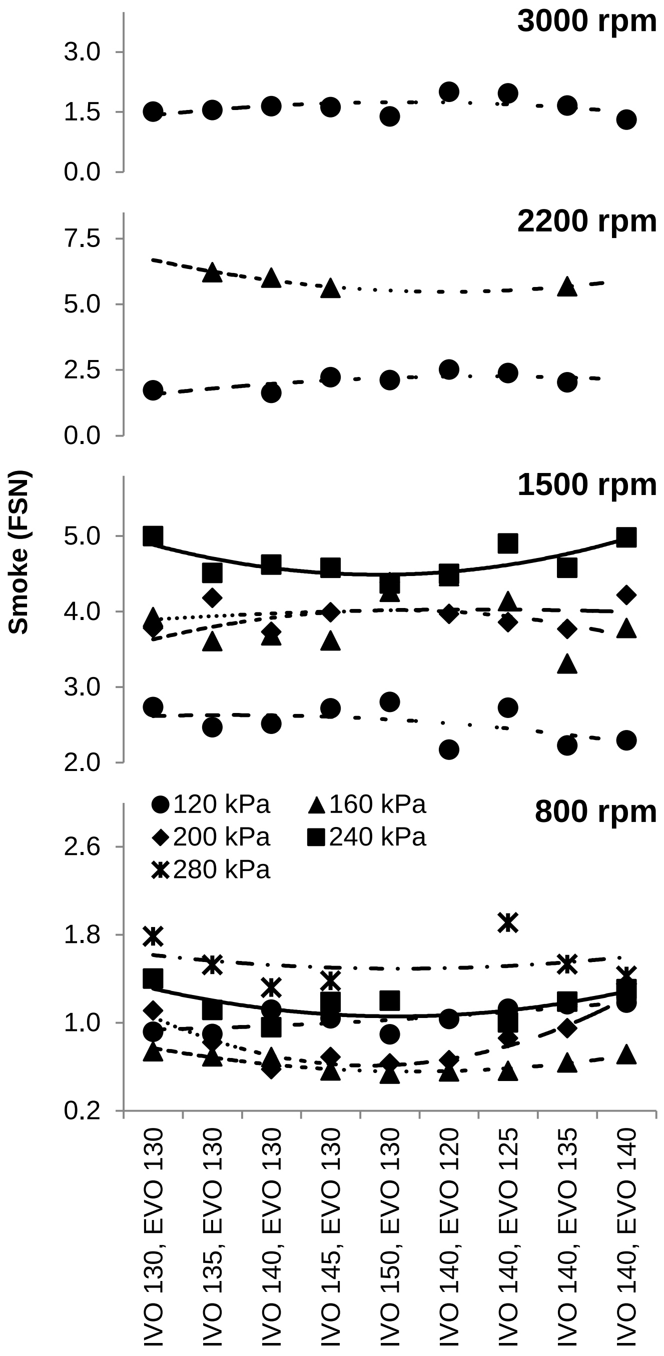

Figure 20 - Smoke emissions

Finally, the NOx emissions are presented in Figure 21. By moving along the x-axis from the middle to both sides, more residual gas was trapped resulted from lower scavenging efficiencies. Because of the increased heat capacity of CO_2 and reduced oxygen availability by the presence of recycled burned gases, the combustion temperature and hence NOx formation were significantly reduced [29].

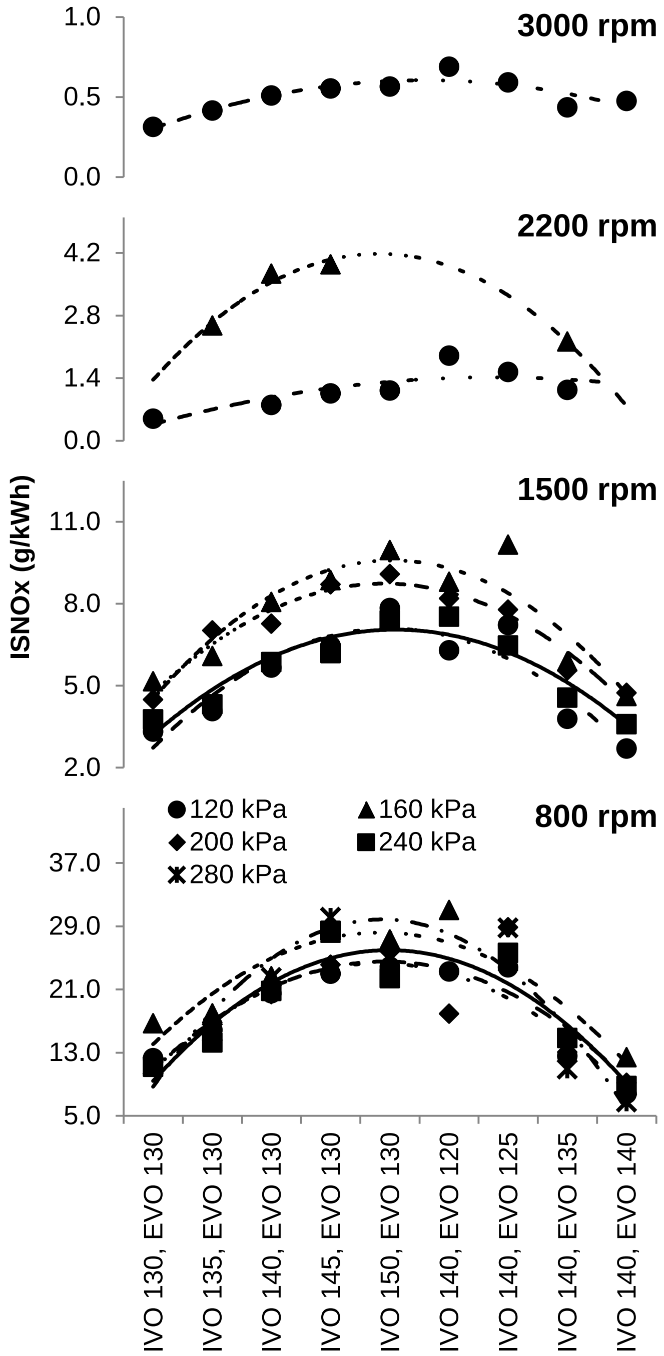

Figure 21 - Oxides of nitrogen emissions

At 800 rpm the early EVO raised the charge oxygen availability, increasing NOx emissions to levels of downsized four-stroke engines operating at similar conditions [30]. As the speed increased from 800 to 3000 rpm, the combustion mode progressed from SI towards CAI as a result of higher levels of hot residual gas trapped. Consequently, the NOx emissions progressively decreased thanks to the higher charge dilution and lower combustion temperature.

From Figure 21 it is also noted that the NOx emissions were more sensitive to the valve timings studied than to the load itself, especially at 800 rpm. At this speed the emissions of oxides of nitrogen increased by 20% as the boost pressure was changed from 120 to 280 kPa (0.66 to 1.22 MPa IMEP). In comparison, by retarding the IVO in 10° CA from 130° to 140° CA ATDC the NOx emissions nearly doubled. The spark timing also played an important role in NOx emissions, as shown by the point “IVO 140, EVO 120” at 200 kPa boost. The ignition timing in this case had to be retarded to avoid knocking combustion (Figure 13), reducing the in-cylinder peak temperature and NOx production.

At 2200 and 3000 rpm and intake pressure of 120 kPa, pure CAI combustion took place. At 2200 rpm the NOx emissions rose rapidly as the boost pressure was increased from 120 kPa to 160 kPa, as a result of both reduced residual gas concentration and presence of high temperature flame in the spark assisted CAI combustion.

4. Conclusions

In this study, a four-valve direct injection gasoline engine was operated in the two-stroke cycle mode by opening both the intake and exhaust valves around BDC. The exhaust gas was scavenged by compressed air during the valve overlap period. At each engine speed and boost pressure, the engine output was measured as a function of intake and exhaust valve timings. The results can be summarised as follows:

- At 800 rpm the peak IMEP of 1.2 MPa was achieved at an intake pressure of 280 kPa, producing a specific torque of 195 Nm/l with the in-cylinder peak pressure as low as 6.8 MPa. At each engine speed, the maximum IMEP was obtained with the highest scavenging efficiency. As the engine speed was increased, the maximum output was limited by the scavenging process and violent heat release rate.

- For the given valve duration and valve lift, the maximum scavenging efficiency of 95% could be achieved at 800rpm. At any given IVO and EVO timings the scavenging efficiency dropped with the increased engine speed due to the reduced time available for the gas exchange process, besides the reduced valve opening area resulted from the hydraulically actuated valves.
- The trapping efficiency increased from about 35% to 70% with higher engine speeds as the air short-circuiting rate was reduced.
- At 800 rpm and 1500rpm the heat release process was dominated by spark ignited flame propagation combustion. At higher engine speeds, CAI combustion took place and the spark timing had no effect whatsoever.
- The ISFC was primarily determined by the combustion efficiency, which was directly related to the in-cylinder air/fuel ratio. The relative air/fuel ratios of the in-cylinder mixture could be increased by optimisation of the valve timings for maximum scavenging efficiency.
- The CO emissions were directly affected by the in-cylinder lambda. At 800rpm, negligible CO emission was measured with optimised valve timings.
- Compared to CO emissions, uHC emissions and exhaust smoke levels were found to be more affected by the fuel impingement and localised over-rich fuel mixtures in the cylinder.
- NOx emissions were found to be very low at higher engine speeds when there was high residual gas concentration and CAI combustion.

The above results have demonstrated that the scavenging process and fuel preparation are the two most important issues affecting the two-stroke poppet valve engine's performance and emissions. The scavenging process can be further optimised by additional experiments with different valve opening duration and timings on the engine. To improve the fuel preparation process, it would be necessary to increase the injection pressures and employ split injections. A more robust stratified charge combustion system design, such as a centrally mounted fast DI injector, would be also desirable.

Acknowledgements

The first author would like to acknowledge the Brazilian council for scientific and technological development (CNPq - Brasil) for supporting his PhD at Brunel University London.

Abbreviations

ATDC: after top dead centre

CA: crank angle

CAI: controlled auto-ignition

CO: carbon monoxide

COV_{IMEP}: covariance of the indicated mean effective pressure

$dP/d\theta$: rate of pressure rise

ECR: effective compression ratio

EER: effective expansion ratio

EGR: exhaust gas recycling

EVC: exhaust valve closing

EVO: exhaust valve opening

GDI: gasoline direct injection

uHC: unburned hydrocarbon

IMEP: indicated mean effective pressure

ISCO: indicated specific carbon monoxide

ISFC: indicated specific fuel consumption

ISuHC: indicated specific unburned hydrocarbon

ISNOx: indicated specific oxides of nitrogen

IVC: intake valve closing

IVO: intake valve opening

LHV: lower heating value

KLS: knock limited spark advance

MBT: minimum spark advance for maximum break torque

NOx: oxides of nitrogen, rpm: revolutions per minute

SACI: spark assisted compression ignition

SI: spark ignition

References

[1] Hooper P R, Al-Shemmeri T, Goodwin M J. Advanced modern low-emission two-stroke cycle engines. Proceedings of the Institution of Mechanical Engineers, Part D: Journal of Automobile Engineering 2011; 225: 1531-1543. http://dx.doi.org/10.1177/0954407011408649.

[2] Hundleby G. Development of a Poppet-Valved Two-Stroke Engine - The Flagship Concept. SAE Technical Paper 1990; 900802. http://dx.doi.org/10.4271/900802.

[3] Kenny R G. Developments in Two-Stroke Cycle Engine Exhaust Emissions, Proceedings of the Institution of Mechanical Engineers, Part D: Journal of Automobile Engineering 1992; 206: 93-106. http://dx.doi.org/10.1243/PIME_PROC_1992_206_165_02.

[4] Blair G. Design and simulation of two-stroke engines. Warrendale: Society of Automotive Engineers; 1996. ISBN 978-1-56091-685-7.

[5] Stokes J, Hundleby G, Lake T, Christie M. Development Experience of a Poppet-Valved Two-Stroke Flagship Engine. SAE Technical Paper 1992; 920778. http://dx.doi.org/10.4271/920778.

[6] Heywood J B, Internal Combustion Engines Fundamentals. New York: McGraw-Hill; 1988. ISBN 978-0071004992.

[7] Nomura K, and Nakamura N. Development of a new two-stroke engine with poppet-valves: Toyota S-2 engine, a new generation of two-stroke engines for the future? Proceedings of the IFP International Seminar, Paris, France, 1993; 53–62.

[8] Knoll R. AVL Two-Stroke Diesel Engine. SAE Technical Paper 1998; 981038. http://dx.doi.org/10.4271/981038.

[9] Nakano M, Sato K, Ukawa H. A Two-Stroke Cycle Gasoline Engine with Poppet Valves on the Cylinder Head. SAE Technical Paper 1990; 901664, http://dx.doi.org/10.4271/901664.

[10] Sementa P, Vaglieco B M, Catapano F. Thermodynamic and optical characterizations of a high performance GDI engine operating in homogeneous and stratified charge mixture conditions fuelled with gasoline and bio-ethanol. Fuel 2012; 96: 204-219. http://dx.doi.org/10.1016/j.fuel.2011.12.068.

[11] Cairns A, Zhao H, Todd A, Aleiferis P. A study of mechanical variable valve operation with gasoline–alcohol fuels in a spark ignition engine. Fuel 2013; 106: 802-813. http://dx.doi.org/10.1016/j.fuel.2012.10.041.

[12] Osborne R, Li G, Sapsford S, Stokes J. et al. Evaluation of HCCI for Future Gasoline Powertrains. SAE Technical Paper 2003; 2003-01-0750. http://dx.doi.org/10.4271/2003-01-0750.

[13] Zhang Y, Zhao H. Investigation of combustion, performance and emission characteristics of 2-stroke and 4-stroke spark ignition and CAI/HCCI operations in a DI gasoline. Applied Energy 2014; 130: 244-255. http://dx.doi.org/10.1016/j.apenergy.2014.05.036.

[14] Pohorelsky L, Brynych P, Macek J, Vallaude P, et al. Air System Conception for a Downsized Two-Stroke Diesel Engine. SAE Technical Paper 2012; 2012-01-0831. http://dx.doi.org/10.4271/2012-01-0831.

[15] Tribotte P, Ravet F, Dugue V, Obernesser P, et al. Two Strokes Diesel Engine - Promising Solution to Reduce CO2 Emissions. Procedia - Social and Behavioural Sciences 2012; 48: 2295-2314. http://dx.doi.org/10.1016/j.sbspro.2012.06.1202.

[16] Martin S, Beidl C, Mueller R. Responsiveness of a 30 bar BMEP 3-Cylinder Engine: Opportunities and Limits of Turbocharged Downsizing. SAE Technical Paper 2014; 2014-01-1646. http://dx.doi.org/10.4271/2014-01-1646.

[17] Eichhorn A, Lejsek D, Hettinger A, Kufferath A. Challenge Determining a Combustion System Concept for Downsized SI-engines - Comparison and Evaluation of Several Options for a Boosted 2-cylinder SI-engine. SAE Technical Paper 2013; 2013-01-1730. http://dx.doi.org/10.4271/2013-01-1730.

[18] Zhang Y, Zhao H, Ojapah M, Cairns A. CAI combustion of gasoline and its mixture with ethanol in a 2-stroke poppet valve DI gasoline engine. Fuel 2013; 109: 661-668. http://dx.doi.org/10.1016/j.fuel.2013.03.002.

[19] Osborne R, Stokes J, Lake T, Carden P, et al. Development of a Two-Stroke/Four-Stroke Switching Gasoline Engine - The 2/4SIGHT Concept. SAE Technical Paper 2005; 2005-01-1137. http://dx.doi.org/10.4271/2005-01-1137.

[20] Sadakane S, Sugiyama M, Kishi H, Abe S, et al. Development of a New V-6 High Performance Stoichiometric Gasoline Direct Injection Engine. SAE Technical Paper 2005; 2005-01-1152. http://dx.doi.org/10.4271/2005-01-1152.

[21] Stone R. Introduction to internal combustion engines. 4th ed. Basingstoke: Palgrave Macmillan; 2012. ISBN 978-0230576636.

[22] Zhang Y, Ojapah M, Cairns A, Zhao H. 2-Stroke CAI Combustion Operation in a GDI Engine with Poppet Valves. SAE Technical Paper 2012; 2012-01-1118. http://dx.doi.org/10.4271/2012-01-1118.

[23] United Nations Regulation 49. Uniform provisions concerning the measures to be taken against the emission of gaseous and particulate pollutants from compression-ignition engines and positive ignition engines for use in vehicles. Official Journal of the European Union; 2013. http://eur-lex.europa.eu/legal-content/EN/TXT/?uri=CELEX:42013X0624(01).

[24] Xu R. A Convenient Technique for Determining Two-Stroke Emissions Measurements Accuracy and A/F Ratio. SAE Technical Paper 1996; 961804. http://dx.doi.org/10.4271/961804.

[25] Douglas R. AFR and Emissions Calculations for Two-Stroke Cycle Engines. SAE Technical Paper 1990; 901599. http://dx.doi.org/10.4271/901599.

[26] Wang Z, Qi Y, He X, Wang J, Shuai S, Law C K. Analysis of pre-ignition to super-knock: Hotspot-induced deflagration to detonation. Fuel 2015; 144: 222-227. http://dx.doi.org/10.1016/j.fuel.2014.12.061.

[27] Benson R S, Brandham P T. A method for obtaining a quantitative assessment of the influence of charging efficiency on two-stroke engine performance. International Journal of Mechanical Sciences 1969; 11: 303-312. http://dx.doi.org/10.1016/0020-7403(69)90048-4.

[28] Li L, Xie H, Chen T, Yu W, et al. Experimental Study on Spark Assisted Compression Ignition (SACI) Combustion with Positive Valve Overlap in a HCCI Gasoline Engine. SAE Technical Paper 2012; 2012-01-1126. http://dx.doi.org/10.4271/2012-01-1126.

[29] Zhao H. HCCI and CAI engines for the automotive industry. Cambridge: Woodhead Publishing; 2007. ISBN 978-1-84569-128-8.

[30] Zhao H. Advanced Direct Injection Combustion Engine Technologies and Development Vol 1. Cambridge: Woodhead Publishing; 2010. ISBN 9781845693893.